Mon. Not. R. Astron. Soc. **000**, 000–000 (0000) Printed 20 December 2001 (MN LATEX style file v2.2)

Molecular hydrogen at $z_{\rm abs} = 1.973$ toward Q 0013−004: Dust depletion pattern in damped Lyman-α systems ⋆

Patrick Petitjean[1,2], R. Srianand[3], & Cedric Ledoux[4]
[1] *Institut d'Astrophysique de Paris - CNRS, 98bis Boulevard Arago, F-75014 Paris, France - email: petitjean@iap.fr*
[2] *LERMA, Observatoire de Paris, 61, avenue de l'Observatoire, F-75014, Paris, France*
[3] *IUCAA, Post Bag 4, Ganeshkhind, Pune 411 007, India - email: anand@iucaa.ernet.in*
[4] *European Southern Observatory, Karl-Schwarzschild Straße 2, D-85748 Garching bei München, Germany - email: cledoux@eso.org*

Typeset 20 December 2001; Received / Accepted

ABSTRACT
We study the dust depletion pattern in different well separated components of the $z_{\rm abs} = 1.973$, log N(H I) = 20.83, damped Lyman-α system toward Q 0013−004. The apparent correlation between [Fe/S] and [Si/S] in the components indicates that the abundance pattern is indeed due to dust-depletion. In particular, we find evidence for depletion similar to what is observed in cold gas of the Galactic disk in one of the weakest components ([Fe/Zn] = −1.62, [Fe/S] = −1.82, [Zn/S] = −0.2, [Si/S] = −0.92) in which molecular hydrogen is detected with log $N(H_2) \sim 16.5$. This is the first time that such depletion is seen in a DLA system. Extinction due to this component is negligible owing to small total HI column density, log N(HI) $\leqslant$ 19.4. This observation supports the possibility that current samples of DLA systems might be biased against the presence of cold and dusty gas along the line of sight.
The global metallicities of this peculiar DLA system in which O I and C II are spread over ∼1050 km s^{-1} are [P/H] = −0.64, [Zn/H] = −0.75 and [S/H] = −0.76 relative to solar. The overall molecular fraction is in the range $-2.7 < \log f < -0.6$. which is the highest value found for DLA systems. H_2 is detected in four components at −625, −475, 0 and 80 km s^{-1} relative to the strongest component at $z_{\rm abs} = 1.97296$. CO is not detected (log N(CO)/N(H I) < −8) and HD could be present at $z_{\rm abs} = 1.97380$. We show that the presence of H_2 is closely related to the physical conditions in the gas: high particle density together with low temperature. Excitation of high J levels and molecular fraction vary largely from one component to the other suggesting that the UV radiation field is highly inhomogeneous through the system. Gas pressure, estimated from C I absorptions, is larger than what is observed in the ISM of our Galaxy. This, together with the complex kinematics, suggests that part of the gas is subject to high compression due to either collapse, merging and/or supernovae explosion. This is probably a consequence of star-formation activity in the vicinity of the absorbing gas.

Key words: *Cosmology:* observations – *Galaxies:* halos – *Galaxies:* ISM – *Quasars:* absorption lines – *Quasars:* individual: Q 0013−004

1 INTRODUCTION

The amount of dust present at high redshift has important consequences on the physics of the gas. In addition, dust directly affects our view of the high redshift universe through extinction. Therefore, the presence of dust in damped Lyman-α (hereafter DLA) systems, that contain most of the neutral hydrogen in the universe, can have significant consequences. Although the presence of dust in damped Lyman-α systems has been claimed very early (Pei et al. 1991), the issue has remained controversial. Indeed, Lu et al. (1996) have questioned the idea that the overabundance of Zn compared to Cr or Fe observed in DLA systems (e.g. Pettini et al. 1997) is due to selective depletion into dust-grains and have argued that the overall metallicity pattern is indicative of Type II supernovae enrichment. In the recent years several studies have shown that both effects,

⋆ Based on observations carried out at the European Southern Observatory (ESO) under prog. ID No. 66.A-0624 and 267.A-5714 with UVES the echelle spectrograph mounted on the Very Large Telescope (VLT) at Cerro Paranal Observatory in Chile.

dust-depletion and peculiar nucleosynthesis history, should be invoked to explain the abundance pattern (Vladilo 1998, Prochaska & Wolfe 1999, Ledoux et al. 2001a). However the lack of statistics and the wide variety of objects that can give rise to DLAs, namely dwarf galaxies (Centurión et al. 2000), large disks (Prochaska & Wolfe 1997, Hou et al. 2001), galactic building blobs (Haehnelt et al. 1998, Ledoux et al. 1998) etc., with, for each of these objects, its own history, prevent us to have a clear picture of the nature of DLAs. Nevertheless, all studies conclude that the dust content of DLA systems is small. However, it is possible that the current sample of DLAs is biased against high-metallicity and dusty systems. Indeed, Boissé et al. (1998) have noticed that there is a lack of systems with large N(H I) and large metallicity. Very recent investigation of an homogeneous sample of radio-selected quasars shows that the dust-induced bias cannot lead to underestimate the H I mass in DLA systems by a large factor (Ellison et al. 2001). However even a factor of two could change our understanding of DLA systems.

An obvious way to search for DLAs with large amounts of dust is to select those where molecules are detected. However, it may not be so simple as it has been shown that the presence of H_2 is not only related to the dust-to-metal ratio but is mostly dependent on the physical conditions of the gas. First of all, H_2 is detected when the particle density is large (Petitjean et al. 2000, Ledoux et al. 2001b). In any case, the system at $z_{abs} = 1.973$ toward Q 0013−004 is a good target as very strong molecular absorptions have been identified by Ge & Bechtold (1997, see also Ge et al. 1997).

2 OBSERVATIONS

The Ultra-violet and Visible Echelle Spectrograph (D'Odorico et al. 2000) mounted on the ESO Kueyen 8.2 m telescope at the Paranal observatory has been used on October 20-23, 2000, to obtain high-spectral resolution spectra of Q 0013−004. Additional observations were performed in service mode in August and September 2001. The slit width was 1 arcsec (the seeing $FWHM$ was most of the time better than 0.8 arcsec) and the CCDs were binned 2×2 resulting in a resolution of ∼45000. The total exposure time ∼20 hours was split into 1 h exposures. Two settings were used to cover the complete wavelength range. The data was reduced in the dedicated context of MIDAS, the ESO data reduction package, using the UVES pipeline in an interactive mode. The main characteristics of the pipeline is to perform a precise inter-order background subtraction for science frames and master flat-fields, and an optimal extraction of the object signal rejecting cosmic ray impacts and subtracting the sky at the same time. The reduction is checked step by step. Wavelengths were corrected to vacuum-heliocentric values and individual 1D spectra were combined together. The resulting S/N ratio per pixel is of the order of 35 at ∼3500 Å and 80 at ∼5000 Å.

3 THE DLA SYSTEM AT $Z_{ABS} = 1.973$

3.1 Molecular hydrogen

The presence of H_2 in the $z_{abs} = 1.973$ system toward Q 0013−004 was first reported by Ge & Bechtold (1997).

Table 1. Fit results for H_2 lines

z_{abs}	Level	log N (cm^{-2})	n_{lines}	T_{ex} (K)
1.96685[a]	J = 0	$2.35\pm0.25 \times 10^{15}$	3	...
	J = 1	$1.21\pm0.19 \times 10^{16}$	2	300^{+276}_{-96}
	J = 2	$6.09\pm1.10 \times 10^{15}$	1	776^{+584}_{-244}
	J = 3	$3.39\pm0.39 \times 10^{15}$	2	382^{+35}_{-29}
	J = 4	$\leqslant 2.5 \times 10^{14}$	...	...
1.96822[b]	J = 0	$1.05\pm0.08 \times 10^{16}$:	1	...
	J = 1	$9.03\pm1.61 \times 10^{15}$	2	73^{+7}_{-8}
	J = 2	$9.65\pm1.30 \times 10^{15}$	1	302^{+33}_{-30}
	J = 3	$4.18\pm0.43 \times 10^{15}$	3	258^{+6}_{-12}
	J = 4	$8.58\pm0.68 \times 10^{14}$	3	363^{+10}_{-12}
	J = 5	$3.57\pm0.42 \times 10^{14}$	5	372^{+9}_{-11}
1.97296[c]	J = 0	5.5×10^{16}–1.0×10^{19}	...	...
	J = 1	1.4×10^{17}–2.0×10^{19}	...	...
	J = 2	7.5×10^{16}–2.0×10^{19}	...	...
	J = 3	4.3×10^{16}–1.0×10^{19}	...	...
	J = 4	$1.46\pm0.56 \times 10^{15}$	...	...
	J = 5	$1.30\pm0.14 \times 10^{15}$	...	...
1.97380[d]	J = 0	5.0×10^{16}–6.0×10^{18}	...	...
	J = 1	1.0×10^{17}–3.0×10^{19}	...	...
	J = 2	5.0×10^{16}–3.0×10^{18}	...	...
	J = 3	$6.42\pm0.91 \times 10^{15}$	1	...
	J = 4	$\leqslant 5 \times 10^{14}$	...	...

[a] $b = 8.89\pm0.46$ km s^{-1}; [b] $b = 7.07\pm0.33$ km s^{-1}
[c] $b = 18.87\pm2.74$ km s^{-1}; [d] $b = 11.26\pm0.93$ km s^{-1}

Based on an intermediate resolution spectrum and a single component curve of growth, they derived a very high value of the molecular fraction, $f = 2\ N(H_2)/[N(H\ I)+2N(H_2)] = 0.22 \pm 0.05$. In the UVES data, H_2 is detected in four distinct main components spread over ∼700 km s^{-1}, at z_{abs}= 1.96685 (∼ −615 km s^{-1}), 1.96822 (∼ −475 km s^{-1}), 1.97296 (0 km s^{-1}) and 1.97380 (∼ +80 km s^{-1}), marked with vertical dotted lines in Fig. 1. For simplicity we name these components **a**, **b**, **c** and **d** respectively. Four additional strong metal components at z_{abs}= 1.96729 (∼ −572 km s^{-1}), 1.97023 (∼ −268 km s^{-1}), 1.97098 (∼ −200 km s^{-1}) and 1.97138 (∼ −159 km s^{-1}), with highly saturated O I, Si II and Mg II lines, *but clearly identified by the weaker S II lines*, are marked with vertical dashed lines in Fig. 1 (see also Fig. 2 and Fig. 4). These additional components, in which we measure a conservative upper limit, $N(H_2) \leqslant 10^{14}$ cm^2, probably have a non-negligible contribution to the total H I column density.

In the case of components **c** and **d** the absorption lines due to $J \leqslant 3$ levels are strongly saturated and possibly blended with other lines. This implies that we can only derive a lower limit on the H_2 column density from the condition that the lines must be saturated and an upper limit from the absence of damping wings. Results are given in Table 1 together with the number of unblended lines, n_{lines}, that are used to derive the column densities.

Components **a** and **b** are narrow and mostly unblended. As the lines are moderately saturated it is possible to derive H_2 column densities for various J levels (see Table 1). The total H_2 column density in these components is $2.39\pm0.22 \times 10^{16}$ and $3.46\pm0.40 \times 10^{16}$ cm^{-2} respectively. The excitation temperatures $T_{01} = 300^{+276}_{-96}$ and 73^{+7}_{-8} K could reflect the kinetic temperature of the gas (e.g. Abgrall et al. 1992).

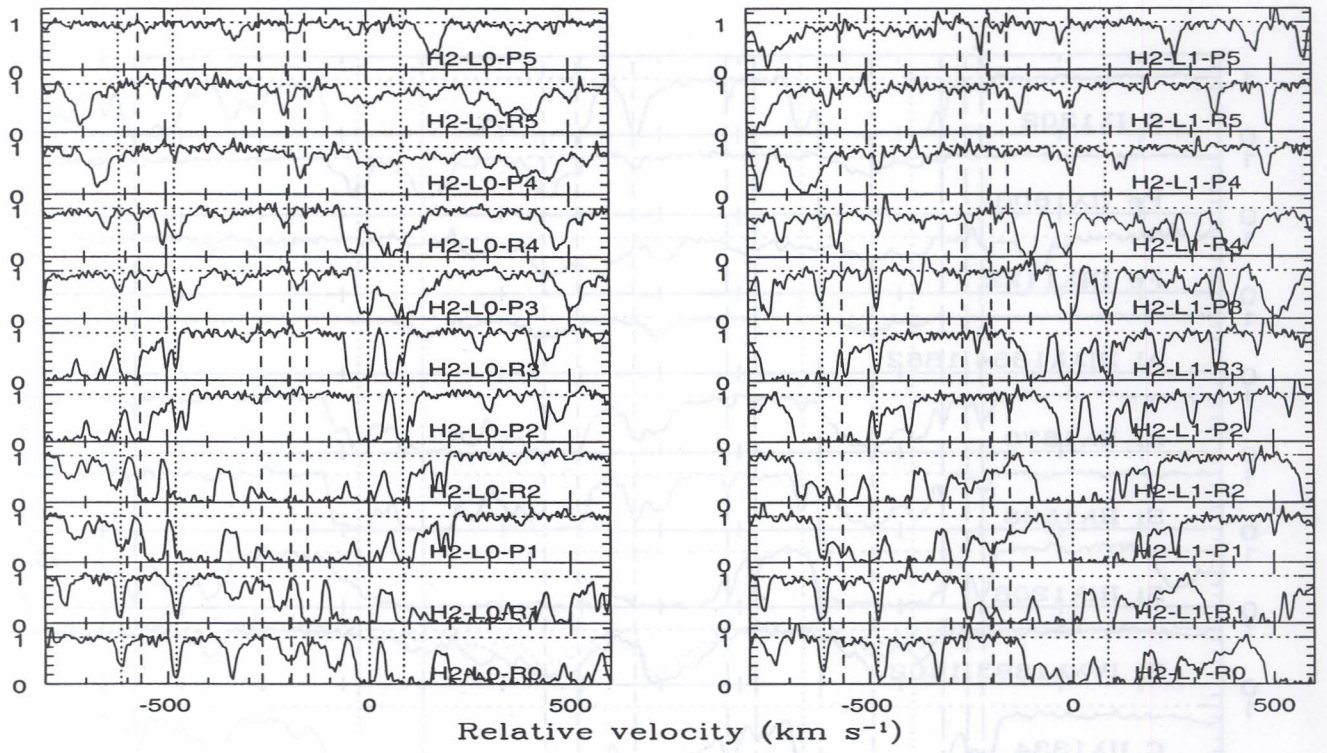

Figure 1. H_2 absorption profiles for transitions from different levels, $v = 1 - 0$ (left panels) and $2 - 0$ (right panels), given on a velocity scale defined with respect to $z_{\rm abs}$= 1.97296. The vertical dotted lines indicate the positions of the four H_2 components discussed in the text. The location of components with strong O I, Si II, Mg II and S II absorption lines but without detectable absorption due to H_2 is indicated by dashed vertical lines.

In the case of component **a** the excitation temperatures for the ortho and para states ($T_{02} = 776^{+584}_{-244}$ K and $T_{13} = 401^{+62}_{-55}$ K) are different (although errors are large). This happens also in component **b**. Note however that the estimated column densities of $J = 0$ and $J = 2$ levels are based on a single unblended line. Moreover, $J = 0$ transitions from this component are blended with $J = 1$ transitions at $z_{\rm abs}$=1.96685 (see Fig. 1). The fact that T_{02} and T_{13} are different indicates that excitation is not dominated by collisions only and other processes such as UV pumping are important (see Srianand & Petitjean 1998). As emphasized by Srianand et al. (2000), populating the J = 4 level after formation of a molecule on a dust-grain is probably negligible in this gas. The photo-absorption rate in the Lyman and Werner bands is therefore $\beta_o \leqslant 10^{-9}$ and $9{\times}10^{-10}$ s^{-1}, respectively, for **a** and **b** based on the $J = 4$ column densities. This is consistent with what is measured in the Galactic ISM.

Absorption due to H_2 is detected up to $J = 5$ in component **c**. The lines from the $J = 4$ and 5 levels are narrow and unsaturated and we used a single component fit to derive the column densities. Neglecting the formation pumping to $J = 4$ and using the lower limit on the $J = 0$ column density, we obtain $\beta_o \leqslant 3.0 \times 10^{-10}$s^{-1}. This is at least a factor 3 smaller than that derived for component **b**.

It is clear from Fig. 1 that the $J \geqslant 4$ lines are either absent or weak in component **d**. We determine the column density for $J = 3$ from the H_2-L_0-R_3 line that is not saturated. Absence of absorption from high J levels, despite strong saturation of the transitions from $J \leqslant 2$ levels, suggests that the rate of UV pumping to high J levels is low in this component. We derive $\beta_o \leqslant 1.1 \times 10^{-10}$s^{-1} which is at least a factor 8 smaller than what is derived for component **b**.
All this indicates that there are large fluctuations of the ambiant UV flux inside the system.

3.2 Atomic hydrogen

The overall structure of the strong metal lines is illustrated in Fig. 2. The location of the strongest components with and without detected H_2 molecules is indicated by, respectively, dotted and short-dashed lines as in Fig. 1. The long-dashed lines show components with absorption due to low-ionization species only. It can be seen that the low-ionization absorptions (from O I, C II, Si II, Mg II) span about 1000 km s^{-1} and are structured in two main strong systems at $z_{\rm abs} \sim 1.9676$ and 1.9733 separated by 575 km s^{-1}. Note that most of the Si IV and C IV absorption is located inbetween these two strong low-ionization systems.
A Voigt profile centered at the mean position of the two strongest H_2 components, $z_{\rm abs} = 1.9733$, gives a good fit to the red wing of the Lyman-α absorption with a total column density, N(H I) = $6.7{\times}10^{20}$ cm^{-2}. This is consistent with that derived by Ge & Bechtold (1997). There is however an excess of absorption in the blue wing that we attribute to the second system and in particular the H_2 components **a**

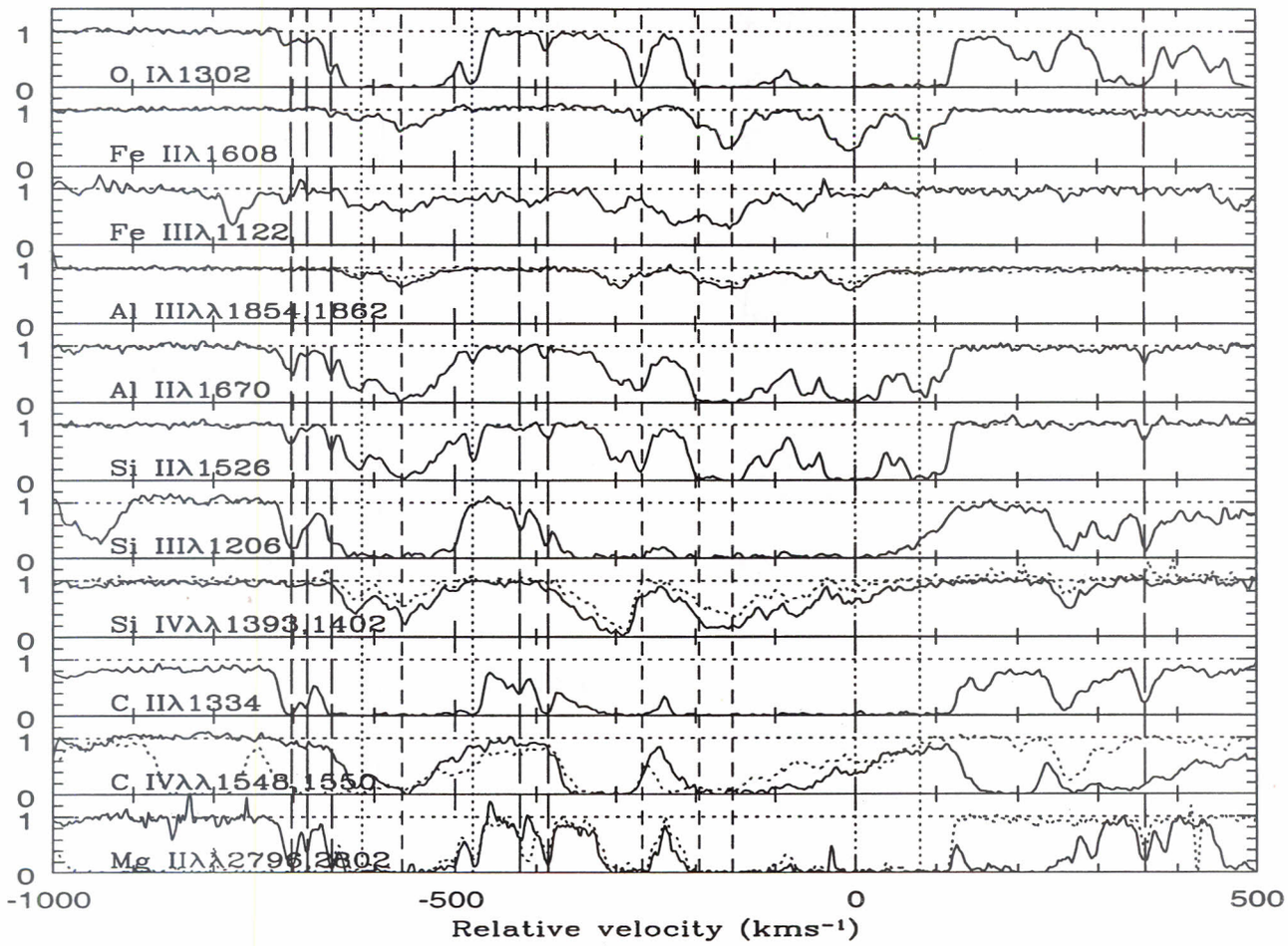

Figure 2. Metal line profiles on a velocity scale with origin at redshift $z_{\rm abs} = 1.96822$. The vertical dotted and short-dashed lines are as in Fig. 1. The vertical long-dashed lines emphasize narrow components seen only in low-ionization species. For doublets, profiles of the weakest line is overplotted as a dashed line.

and **b** that are blue-shifted by 615 and 475 km s^{-1} relative to the strongest H_2 component. We can therefore estimate N(H I) associated with these two blueshifted components. In Fig. 3 we show the fit of the continuum in the region of interest (top panel) and the fits to the damped absorption (bottom panel) with and without the additional absorption (log N(H I) = 19.4) that can be accomodated at $z_{\rm abs} \sim 1.96753$. This implies that less than 10% of the HI gas is associated with H_2 components **a** and **b**. This gives a lower limit on the molecular fraction $f > 2 \times 10^{-3}$ and 4×10^{-3} for components **a** and **b** respectively. These limits are higher than what has been observed in other damped systems (e.g. Petitjean et al. 2000). Such a large value for f in a low HI column density cloud is at odd with what is observed in the ISM of our Galaxy where log $f < -4$ for log N(H I) < 20 (Savage et al. 1977). This implies high formation rate, and therefore large amount of dust, high density, low temperature, *and* low destruction rate, and therefore shielding from the UV field.

We derive for the whole system $6{\times}10^{17} <$ log $N(H_2) < 1{\times}10^{20}$ cm^{-2}. Therefore, the mean fraction of molecular hydrogen is in the range 0.002−0.25. This is much larger than what is seen in other DLA systems (see Petitjean et al. 2000; Ledoux et al. 2001b).

3.3 Other molecules

If the molecular fraction is close to the upper limit we derived above then one can expect to detect other molecular species such as CO and HD (see Varshalovich et al. 2001). We do not detect molecular CO down to $w_{\rm obs}(\lambda 1088) < 7$ mÅ. This means $N(\rm CO) < 2{\times}10^{12}$ cm^{-2} in components **c** and **d**, using the oscillator strength by Morton (1975). Therefore log $N(\rm CO)/N(H\ I) < -8.5$. Note that in our Galaxy, when log $N(H_2) > 19$, CO is readily detected with log $N(\rm CO) \geqslant 13$ (Federman et al. 1980).

It is difficult to trace HD in this system because blending of lines is severe for all bands. At $z_{\rm abs} = 1.97296$ (component **c**), absorption features are present at the expected position of HD-L0-R0 and HD-L1-R0 but they are stronger than a possible HD-L3-R0 absorption ($w_{\rm obs} \sim 30$ mÅ). Note that consistent features are seen at $z_{\rm abs} = 1.97278$, espe-

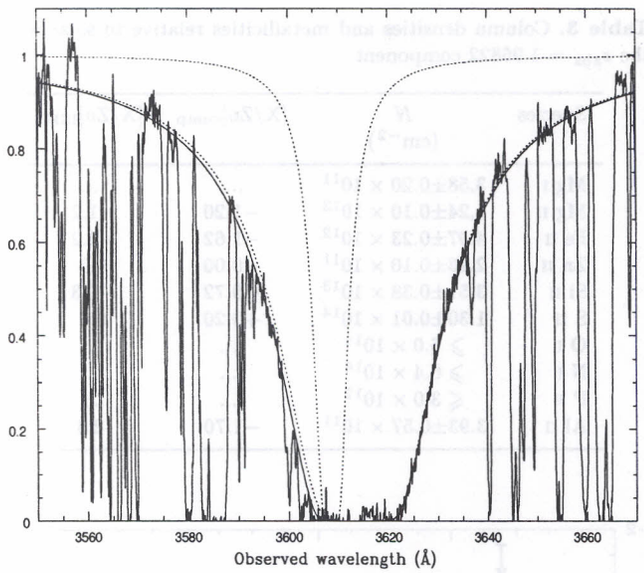

Figure 3. Fits of the damped Lyα absorption profile at $z_{abs} = 1.9733$. Fits with (solid line) and without (dotted line) the maximum column density (log N(H I = 19.4) in the component at $z_{abs} = 1.96822$, compatible with the asymmetry of the profile.

cially at the expected position of HD-L3-R0 but HD-L0-R0 is not visible down to $w_{obs} < 40$ mÅ. The large equivalent width limit is a consequence of the line falling in the wing of another stronger absorption. At $z_{abs} = 1.97380$ (corresponding to component **d**), consistent absorption features are present at the expected position of HD-L0-R0, HD-L3-R0 and HD-L4-R0. HD-L1-R0 is possibly present but blended. The detection should be considered as tentative as HD-L0-R0 and HD-L3-R0 are affected by noise. The strongest constraint on this component is given by w_{obs}(HD-L0-R0) $\sim$ 10 mÅ. Using $\lambda = 1105.845$ and $f = 7.6\times10^{-4}$ we derive N(HD) $\sim 4\times10^{14}$ cm^{-2}. Using the limits on H_2 indicated in Table 1, we derive $1.0\times10^{-5} < N(HD)/N(H_2) < 2\times10^{-3}$.

4 METALLICITY AND DEPLETION

4.1 The system as a whole

The absorption lines from heavy elements show a complex multiple component structure (see Fig. 4) and only a few of the strong velocity components have detectable associated H_2 absorption.

The column densities of different species, integrated over, respectively, the DLA at $z_{abs} = 1.9733$ and the sub-DLA at at $z_{abs} = 1.96753$ are given in Table 2. For the sub-DLA, we have considered that most of the neutral hydrogen is associated with the two molecular components **a** and **b**. The column densities indicated in Table 2 are therefore the sum of the column densities measured in these two components. Note that the measurements are obtained using transitions with little saturation (see Fig. 4). We use in the following the standard notation [X/H] = log[Z(X)]-log[$Z_\odot$(X)] with

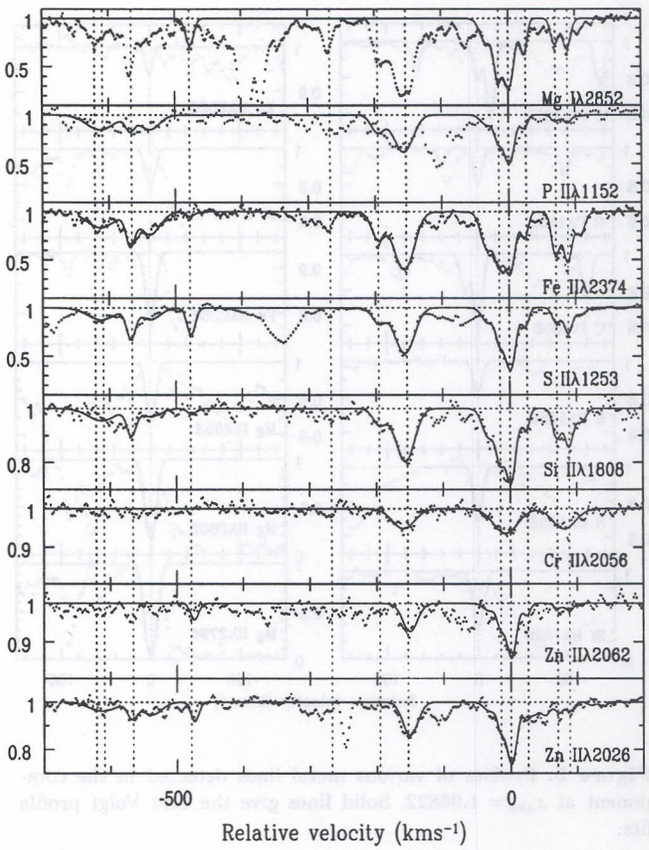

Figure 4. Profiles of various metal lines detected in the DLA system plotted on a velocity scale with origin at $z_{abs} = 1.97296$. Solid lines give the best Voigt profile fits. Vertical dotted lines indicate the positions of subcomponents.

Table 2. Total column densities and metallicities relative to solar

Ion	N (cm^{-2})	[X/S][a,b] DLA	Cold	Warm	Halo
	DLA at $z_{abs} = 1.9733$[c]				
H I	$6.70\pm0.10\times10^{20}$	.....	.....	.....	.....
Si II	$2.70\pm0.20\times10^{15}$	−0.19	−1.3	−0.4	−0.3
S II	$1.90\pm0.10\times10^{15}$	−0.00	....	+0.0	+0.0
P II	$5.71\pm0.77\times10^{13}$	+0.12	−0.5	−0.2	−0.1
Zn II	$5.47\pm0.50\times10^{12}$	+0.01	−0.4	−0.2	−0.1
Cr II	$9.86\pm0.30\times10^{12}$	−0.76	−2.1	−1.2	−0.4
Fe II	$6.41\pm0.46\times10^{14}$	−0.77	−2.2	−1.4	−0.6
Ni II	$1.44\pm0.60\times10^{13}$	−1.15	−2.2	−1.4	−0.6
Mn II	$2.88\pm0.70\times10^{13}$	−1.13	−1.5	−1.0	−0.7
	Sub-DLA at $z_{abs} = 1.96753$[d]				
H I	$<2.70\pm0.20\times10^{19}$	....			
Si II	$2.65\pm0.31\times10^{14}$	−0.38			
S II	$3.32\pm0.29\times10^{14}$	−0.00			
P II	$1.16\pm0.17\times10^{13}$	+0.24			
Zn II	$1.16\pm0.12\times10^{12}$	+0.16			
Fe II	$5.43\pm0.35\times10^{13}$	−1.03			

[a] [X/H] = log[Z(X)]-log[$Z_\odot$(X)]
[b] Galactic values are from Welty et al. (1999)
[c] [S/H] = −0.76 in the DLA system
[d] Components **a** and **b**; [S/H] > −0.12

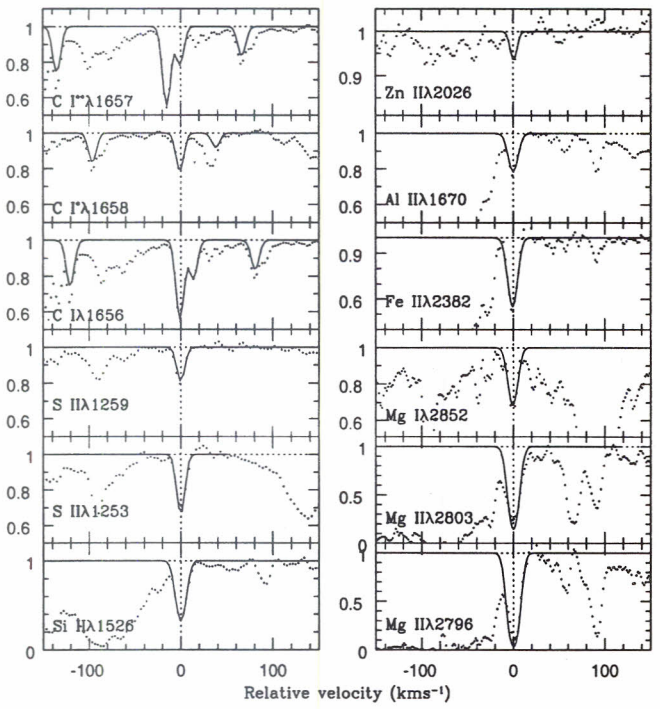

Figure 5. Profiles of various metal lines detected in the component at $z_{\rm abs}$= 1.96822. Solid lines give the best Voigt profile fits.

Z(X) the metallicity of species X. Solar metallicity are from Savage & Sembach (1996).

Sulphur and zinc are not much depleted into dust-grains in the ISM of our Galaxy and therefore are good indicators of metallicity. They have consistent metallicities, about 0.2 solar in the DLA and 0.75 solar in the sub-DLA. Phosphorus is slightly enhanced ($\leqslant$ 1.5 times) compared to Sulphur and zinc in both cases. Iron, Chromium, Nickel and Manganese are underabundant with respect to zinc probably because they are depleted into dust-grains.

It is interesting to note that the abundance pattern seen in the DLA is close to that of warm halo gas whereas the pattern in the sub-DLA is close to that of warm neutral gas in the ISM (see however next Section). This is consistent with the conclusion by Petitjean et al. (2000) that most of the bulk of the DLA population is drawn from warm gas.

4.2 Dust depletion in the $z_{\rm abs}$ = 1.96822 component

In contrast to what is seen for the system as a whole in which absorption by Fe II is strong compared to absorption by Zn II, it is stricking to note that in the $z_{\rm abs}$ = 1.96822 component (H_2 component **b**), the absorption in the strongest iron transigion Fe IIλ2382 has about the same strength as that in Zn IIλ2026 (see Fig. 5). In fact, all transitions from refractory elements are weak. Note that Si III absorption is clearly absent (see Fig. 4), indicating negligible ionization correction. The results of Voigt profile fits to the available metal lines are given in Table 3. Abundances of Zn and S are similar. As can be seen from Table 3, Fe and Al are depleted compared to Zn by two orders of magnitude; Mg and Si are depleted by an order of magnitude compared to S. This is the first time that such a large depletion, consistent with that observed in the cold interstellar medium of the Galactic disk, is observed in a DLA system.

Table 3. Column densities and metallicities relative to solar in the $z_{\rm abs}$ = 1.96822 component

Species	N (cm^{-2})	[X/Zn]$_{\rm comp}$	[X/Zn]$_{\rm ISM}$
Mg I	$3.58\pm0.20 \times 10^{11}$	....	....
Mg II	$1.24\pm0.10 \times 10^{13}$	−1.20	−1.2
Fe II	$4.07\pm0.23 \times 10^{12}$	−1.62	−2.2
Zn II	$2.23\pm0.10 \times 10^{11}$	−0.00	0.0
Si II	$3.51\pm0.38 \times 10^{13}$	−0.72	−1.3
S II	$1.30\pm0.01 \times 10^{14}$	+0.20	0.0
O I	$\geqslant 6.0 \times 10^{14}$	....	....
N I	$\geqslant 6.4 \times 10^{14}$	....	....
P II	$\leqslant 3.0 \times 10^{12}$	....	....
Al II	$3.93\pm0.57 \times 10^{11}$	−1.70	-2.4

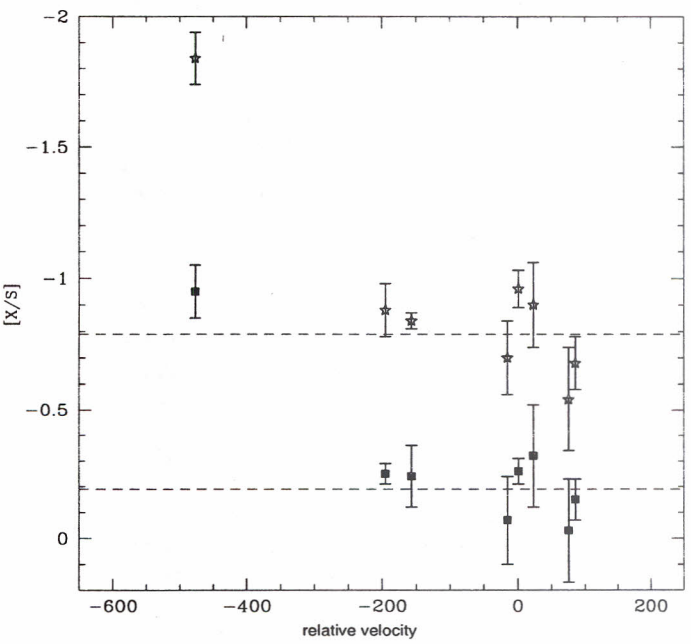

Figure 6. Depletion of Fe (stars) and Si (squares) with respect to S observed in different velocity components. The zero of the velocity scale is at, $z_{\rm abs}$ = 1.97296. The values averaged over the components are indicated by horizontal dashed lines. Note that [Zn/S] in different components is consistent with the solar value within the measurement uncertainties.

4.3 Variations of dust-depletion within the system

We investigate here the variations of the abundance ratios among different well separated velocity components where ionization correction is negligible. This is the case for the components where H_2 is detected. However, heavy element absorption from component **a** is blended with absorption due

to a nearby high ionization features (see Fig 4). Thus we do not consider this component for the analysis. In addition, we consider the two components at ~ 153 and 195 km s^{-1}that account for 20 to 30% of the observed heavy element column densities.

We note that the [Zn/S] ratio is very close to solar (uncertainties are typically of the order of 0.1 dex) in all components. Si and Fe abundances with respect to S are plotted in Fig. 6 for different velocity components. Depletion of Si and Fe is apparent. All components, except the very special component **b** (at -475 km s^{-1} see previous Section), have similar abundance ratios (and therefore depletion factors), irrespective of whether H_2 molecules are present or not. This has already been noted in the $z_{\rm abs} = 1.962$ DLA system toward Q 0551−366 (Ledoux et al. 2001b).

In Fig. 7, [Si/S] is plotted as a function of [Fe/S] as observed in the sub-components. It is apparent from the figure that there is a strong correlation between the two quantities. Note that the correlation is present (albeit with lower significance level) even if we do not consider the $z_{\rm abs} = 1.96822$ component. This clearly demonstrates the existence of differential dust-depletion in a single DLA system. The depletion factors for three gaseous components of our Galaxy are overplotted on Fig. 7: the cold and warm ISM and the halo gas (Welty et al. 1999). It is clear that most of the velocity components have depletion patterns very close to that seen in warm and halo gas in our Galaxy. Only the $z_{\rm abs} = 1.96822$ component has a similar pattern as that of the cold ISM phase.

It is important to note that the lowest depletion factor is recorded in component **d** (at +80 km s^{-1}) that has high H_2 content. In addition, components with similar dust-depletion factors can have very different H_2 contents. This means that the presence of dust, though important to form H_2 molecules at low temperature, is only one of the parameters, together with high particle density and low UV-flux, that decide what is the molecular fraction in the gas.

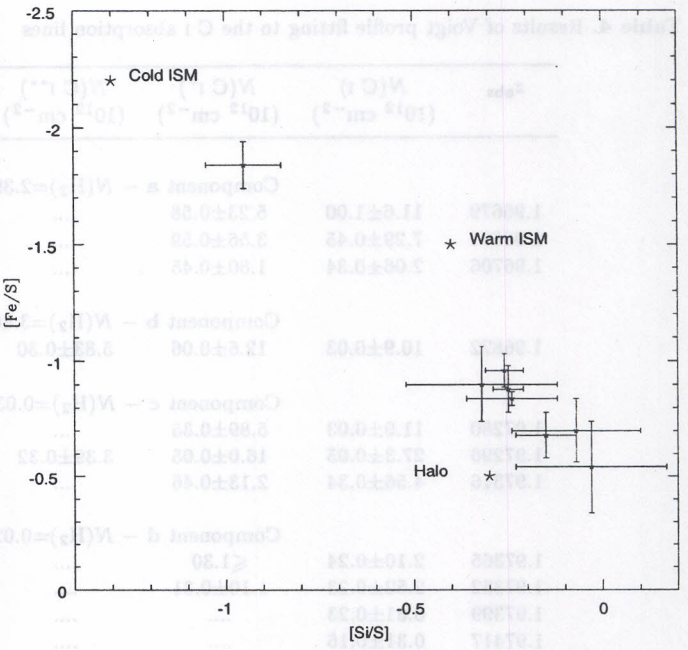

Figure 7. [Fe/S] vs [Si/S] for different velocity components. The corresponding values measured in different gas components in our Galaxy are indicated by stars.

5 PHYSICAL CONDITIONS IN THE GAS

C I is usually seen in components where H_2 is detected (see however Srianand & Petitjean 1998) and it is possible to derive constraints on the particle density of the gas from the relative populations of the different levels of the C I ground term.

Absorption lines produced by C I and C I* are clearly seen in the four components where H_2 is detected. However, C I** is seen only in two components at $z_{\rm abs} = 1.96822$ and 1.97296. In addition, there are three components that show C I absorption without detectable H_2 ($\leqslant 10^{14}$cm^{-2}, see also Srianand & Petitjean 2001). We perform simultaneous Voigt profile fits to the $\lambda_{\rm r} = 1560$ and 1656 Å C I, C I* and C I** lines. The fit results are shown in Fig 8 and summarized in Table 4.

Upper limits on the CMBR temperature, $T_{\rm CMBR}$, are derived assuming that CMBR pumping is the only excitation mechanism. Results, given in column #7 of Table 4, are consistently larger than the value expected from standard hot big-bang model ($\sim$ 8 K, see Srianand et al. 2000). This is because other excitation processes are at play and in particular collisions. We estimate the particle density in the cloud assuming, $T_{\rm CMBR} = 8$ K, $T_{\rm kin} = 100$ K and neglecting fluorescence. The range given are obtained using 2σ uncertainties in the column density estimation. Results are given in column #8 of Table 4.

As the ionization potential of C I is similar to the energy of photons in the molecular bands, it is expected that C I and H_2 follow each other. It is therefore interesting to note that N(C I) in component **d** is about a factor of 2 smaller than in component **b** whereas $N(H_2)$ is at least a factor of ten larger. This is probably a consequence of much larger $N(H_2)/N(H\,I)$ ratio in component **d**, a conclusion supported by the low value of N(S II) in this component (see Table 5). C I, C I* and C I** are clearly detected in component **b** (see Fig 5). The excitation temperature of the $J = 1$ H_2 level is in the range 60-80 K. Assuming that the kinetic temperature has the same value implies that the particle density is in the range $n_{\rm H} = 170$-200 cm^{-3} (with $T_{\rm CMBR} = 8$ K).

It is interesting to note that the components at $z_{\rm abs} = 1.96737$, and 1.96763 have large pressure. Considering the kinetic temperature to be 100 K implies $P/k = 4000 - 13500$ and $2000 - 18000$ cm^{-3}K respectively. However, these components belong to the strong saturated absorption at ~ -600 km s^{-1} (see Fig. 2) that also shows large O I and Si III absorption and no H_2. It is most likely that the temperature of the gas is higher than what we use here (see Petitjean et al. 2000). For $T = 1000$ K, we derive $n = 10$–75 cm^{-3} and 28–54 cm^{-3}, and $P/k = 18,000 - 61,000$ and $10,000 - 75,000$ cm^{-3}K respectively for the two components.

Such high pressures are seen in about one third of the C I gas in our galaxy (see Jenkins & Tripp 2001). This probably indicates that part of the gas in the system under consideration is subject to high compression due to either collapse,

Table 4. Results of Voigt profile fitting to the C I absorption lines

z_{abs}	N(C I) (10^{12} cm^{-2})	N(C I*) (10^{12} cm^{-2})	N(C I**) (10^{12} cm^{-2})	b (km s^{-1})	N(S II) (10^{14} cm^{-2})	T_{CMBR} (K)	n_H (cm^{-3})
		Component **a** – $N(H_2)$=2.39±0.22 × 10^{16} cm^{-2}					
1.96679	11.6±1.00	5.23±0.58	....	3.10±0.57	1.87±0.20	⩽13.8	20-70
1.96691	7.29±0.45	3.56±0.59	....	3.01±0.20	....	⩽14.5	20-80
1.96706	2.06±0.34	1.80±0.45	....	4.93±1.44	....	....	....
		Component **b** – $N(H_2)$=3.46±0.40 × 10^{16} cm^{-2}					
1.96822	10.9±0.03	12.6±0.06	5.83±0.30	4.30±0.20	1.44±0.06	⩽20.0	170-200
		Component **c** – $N(H_2)$=0.03–6 × 10^{19} cm^{-2}					
1.97280	11.9±0.03	5.89±0.35	....	5.98±0.28	1.42±0.18	⩽13.0	40-60
1.97296	27.3±0.05	16.0±0.05	3.39±0.32	6.23±0.16	5.68±0.34	⩽13.5	50-65
1.97316	4.56±0.34	2.13±0.46	....	7.00±0.77	0.82±0.01	⩽15.0	10-85
		Component **d** – $N(H_2)$=0.02–4 × 10^{19} cm^{-2}					
1.97365	2.10±0.24	⩽1.30	....	5.66±0.41	0.73±0.13	⩽15.0	⩽ 85
1.97382	2.52±0.23	1.10±0.31	....	4.52±0.42	1.32±0.15	⩽15.5	⩽ 95
1.97399	0.81±0.23	....	....	7.30±1.02	....	....	....
1.97417	0.31±0.16	....	....	0.371±0.27	....	....	....
		Components with $N(H_2)$⩽ 10^{14}cm^{-2}					
1.96737	8.15±0.63	5.91±0.79	....	14.41±1.08	1.72±0.19	⩽ 17.5	40-135
1.96763	7.08±0.83	4.76±0.99	....	27.14±3.38	1.33±0.20	⩽ 19.3	20-180
1.97109	1.90±0.12	⩽1.30	....	10.05±.91	.....	⩽ 21.0	⩽ 200
1.97144	9.10±.62	8.05±0.60	....	13.44±0.96	....	⩽8.5	65-160

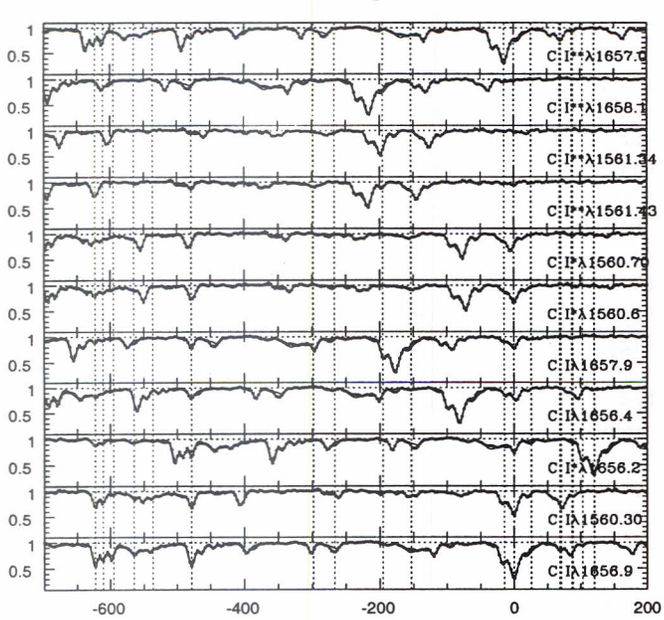

Figure 8. Velocity plot showing the absorption produced by different states of C I. The continuous curve gives the best fitted profile for multiple components.

merging and/or SN explosion. The overall velocity structure of the system at z_{abs} = 1.9676 with the presence of molecular gas at +100 and −150 km s^{-1} from the center of the high ionization gas strongly suggests the expansion of a spherical shell. In any case, intense star-formation activity is occuring in the vicinity of the gas.

6 CONCLUSION

The DLA system at z_{abs} = 1.973 toward Q 0013−004 is peculiar in several aspects. Absorptions from metals are spread over about 1000 km s^{-1}; in particular O I and C II span 1050 km s^{-1}. The velocity structure indicates the presence of two main systems centered at $z \sim 1.973$ and 1.9674, separated by $\sim$ 550 km s^{-1} with, respectively, log N(H I) = 20.83 and <19.4 and [S/H] = −0.76 and > −0.12.

The low-ionization gas is conspicuous in the system. There is clear evidence that all species are at most twice ionized in the z_{abs} = 1.96822 component. This means that if photo-ionization dominates, there is probably very few photons with energy larger than 20 eV. More generally, $N(X^+)/N(X^{2+}) > 1$ over the entire $z \sim 1.973$ system. This ionization state could reveal gas ionized by slow shocks. This idea is reinforced by the high pressure measured in a few components from C I absorptions.

H_2 is detected in four main components, two very strong components (log $N(H_2) > 17$) in the $z \sim 1.973$ system and two weaker components (log $N(H_2) \sim 16$) in the $z \sim 1.9674$ system. The total column density is $17.8 <$ log $N(H_2) < 20.0$ and therefore the mean molecular fraction, $f = 2N(H_2)/(2N(H_2) + N(H\ I))$, is in the range $-2.7 <$ log $f < -0.6$ which is the highest molecular fraction observed in DLA systems.

The analysis of the N(C I*)/N(C I) ratio in different components indicates that whenever H_2 is detected, the particle density is high ($n_H > 30$ cm^{-3}). High density is also

found for gas components without any associated H_2 detected. There is a hint for the depletion within the components to be correlated to the $N(\mathrm{C\ I^*})/N(\mathrm{C\ I})$ ratio. This suggests that depletion could be larger for denser gas.

The component at $z_{\rm abs} = 1.96822$ shows evidence for large depletion of iron and silicon relative to sulfur and zinc ([Fe/Zn] = −1.92, [Fe/S] = −1.86, [Si/Zn] = −1.01, [Si/S] = −0.95) similar to what is observed in cold gas of the Galactic disk. The corresponding dust-extinction is small in this case because, although H_2 is detected with $\log N(H_2) \sim 16.5$, the H I column density is small, $\log N(\mathrm{H\ I}) < 19.4$, in the component. This is direct evidence for a considerable fraction of heavy elements beeing locked into dust-grains, and, as a consequence, this supports the idea that the current sample of DLA systems might be biased against the presence of cold and dusty gas along the line of sight. Note that the rest of the gas shows a depletion pattern close to that of warm gas in the Galactic halo.

The overall kinematics of the system with the two strong sub-systems separated by 550 km s^{-1} suggests that the line of sight is passing through one or several objects in strong interaction. The velocity structure of the system at $z_{\rm abs} = 1.9676$ with the presence of molecular gas at +100 and −150 km s^{-1} from the center of the high ionization absorptions strongly suggests the expansion of a spherical shell. All this, together with the strong inhomogeneity of the UV field, the high pressure in the gas and the high metallicities stongly suggests that intense star-formation activity is occuring in the vicinity of the system which should be revealed by deep imaging in the field.

ACKNOWLEDGMENTS

We gratefully acknowledge support from the Indo-French Centre for the Promotion of Advanced Research (Centre Franco-Indien pour la Promotion de la Recherche Avancée) under contract No. 1710-1. This work was supported in part by the European Communities RTN network "The Physics of the Intergalactic Medium". RS thanks the Institute of Astronomy in Cambridge and the Institut d'Astrophysique de Paris for hospitality during the time part of this work was completed.

REFERENCES

Abgrall, H., Le Bourlot, J., Pineau des Forêts, G., et al. 1992, A&A, 253, 525
Boissé, P., Le Brun, V., Bergeron, J., & Deharveng, J. M. 1998, A&A, 333, 841
Centurión, M., Bonifacio, P., Molaro, P., & Vladilo, G. 2000, ApJ, 536, 540
D'Odorico, S., Cristiani, S., Dekker, H., et al. 2000, Proc. SPIE Vol. 4005, p. 121
Ellison, S. L., Yan, L., Hook, I. M., Pettini, M., Wall, J. V., & Shaver, P. 2001, A&A 379, 393
Federman, S. R., Glassgold, A. E., Jenkins, E. B., & Shaya, E. J. 1980, ApJ, 242, 545
Ge, J., & Bechtold, J. 1997, ApJ, 477, L73
Ge, J., Bechtold, J., & Black, J. H. 1997, ApJ, 474, 67
Haehnelt, M. G., Steinmetz, M., & Rauch, M. 1998, ApJ, 495, 647
Hou, J. L., Boissier, S., & Prantzos, N. 2001, A&A 370, 23
Jenkins, E. B., & Tripp, T. M. 2001, astro-ph/0107177
Ledoux, C., Bergeron, J., & Petitjean, P. 2001a, submitted
Ledoux, C., Srianand, R., & Petitjean, P. 2001b, submitted
Ledoux, C., Petitjean, P., Bergeron, J., Wampler, E. J., & Srianand, R. 1998, A&A, 337, 51
Lu, L., Sargent, W. L. W., Barlow, T. A., Churchill, C. W., & Vogt, S. S. 1996, ApJS, 107, 475
Morton, D.M. 1975, ApJ, 197, 85
Pei, Y. C., Fall, S. M., & Bechtold, J. 1991, ApJ, 378, 6
Petitjean, P., Srianand, R., & Ledoux, C. 2000, A&A 364, L26
Pettini, M., Smith, L.J., King, D. L., & Hunstead, R. W. 1997, ApJ, 486, 665
Prochaska, J. X., & Wolfe, A. M. 1997, ApJ, 474, 140
Prochaska, J. X., & Wolfe, A. M. 1999, ApJS, 121, 369
Savage, B. D., Bohlin, R. C., Drake, J. F., & Budich, W. 1977, ApJ, 216, 291
Savage, B. D., & Sembach, K. R., 1996, ARA&A, 34, 279
Srianand, R., & Petitjean, P. 1998, A&A, 335, 33
Srianand, R., & Petitjean, P. 2001, A&A, 373, 816
Srianand, R., Petitjean, P., & Ledoux, C. 2000, Nature, 408, 931
Varshalovich, D., Ivanchik, A., Petitjean, P., Srianand, R., & Ledoux, C. 2001, AstL, 27, 683
Viegas, S. M. 1995, MNRAS, 276, 268
Vladilo, G. 1998, ApJ, 493, 583
Welty, D. E., Hobbs, L. M., Lauroesch, J. T., Morton, D. C., Spitzer, L., York, D. C., 1999, ApJS, 124, 465